

Tri-Resonant Leptogenesis in a Non-Holomorphic Modular A_4 Scotogenic Model

Tapender*  and Surender Verma† 

Department of Physics and Astronomical Science, Central University of Himachal Pradesh,
Dharamshala-176215, INDIA

Abstract

We investigate low-scale baryogenesis *via* tri-resonant leptogenesis within the scotogenic model with a scalar dark matter embedded in a non-holomorphic modular A_4 symmetry framework. We demonstrate that the model naturally accommodates three nearly degenerate right-handed (RH) neutrinos when they are assigned to the triplet representation of A_4 . The near degeneracy originates from treating the symmetric contribution to the Majorana mass matrix, arising from the $\mathbf{3} \otimes \mathbf{3}$ decomposition of A_4 , as a small perturbation to the dominant singlet contribution. Generalized CP (gCP) symmetry is imposed in the model, rendering the complex modulus τ as the sole source of CP violation which is highly constrained by neutrino oscillation data, making the framework highly predictive. In particular, for the inverted hierarchy (IH), the predicted 3σ range of θ_{23} lies in the lower octant close to maximal value while the Dirac CP phase δ_{CP} and the Majorana phase α_{21} are predicted to lie close to 0° or 360° . Also, in this case, predicted values of m_{ee} and $\sum_i m_i$ can be tested and constrained by future neutrinoless double beta decay ($0\nu\beta\beta$) experiments, as well as by cosmological observations, particularly DESI+BAO and Planck data. In fact DESI+BAO disallows IH in the model. We further show that successful baryogenesis can be achieved for both normal hierarchy (NH) and inverted hierarchy (IH) of light neutrino masses with RH neutrino masses as low as 537 GeV rendering this scenario experimentally testable. For NH, RH neutrino mass degeneracy of $\mathcal{O}(10^{-7}-10^{-6})$ is required, while for IH a stronger degeneracy of $\mathcal{O}(10^{-8})$ is needed. Remarkably, in the NH case, successful baryogenesis can occur even in the deep washout regime with decay parameters of $\mathcal{O}(10^5)$ owing to the tri-resonant enhancement of the CP asymmetry and the inclusion of flavor effects.

*tapenderphy@gmail.com

†s_7verma@hpcu.ac.in

1 Introduction

The Standard Model (SM) of particle physics is one of the most successful theories developed to describe the fundamental constituents of nature and their interactions. Despite its remarkable achievements, it is now well established that the SM is incomplete. In particular, it treats neutrinos as massless particles, whereas compelling experimental evidence from neutrino oscillation experiments confirms that neutrinos are massive [1–6]. Furthermore, the SM fails to account for the existence of dark matter in the Universe and cannot explain the observed matter–antimatter asymmetry. To address these shortcomings, the SM is often extended by introducing additional fields and symmetries. One well-motivated extension is the scotogenic model proposed by Ma [7], which provides a unified framework for explaining both the origin of neutrino masses and the nature of dark matter [8–34]. However, generating the observed baryon asymmetry of the Universe through leptogenesis [35–40] within the scotogenic model presents significant challenges, particularly when the relevant mass scale lies at or below the TeV scale. These challenges mainly arise from strong washout effects induced by the large Yukawa couplings required to satisfy neutrino oscillation data. Various mechanisms have been proposed in the literature to circumvent this issue and successfully realize the required baryon asymmetry without extended the scotogenic model [8–21] and with extension [24–26]. One possible approach is to reduce the Yukawa couplings in order to suppress the washout effects. However, this reduction simultaneously diminishes the generated CP asymmetry, thereby resulting in an insufficient lepton asymmetry. This limitation can be overcome by invoking resonant leptogenesis [41–43], where a small mass splitting among the decaying particles enhances the CP asymmetry. Consequently, it becomes possible to identify regions of parameter space where neutrino oscillation data, dark matter relic density constraints, and the observed baryon asymmetry of the Universe can be simultaneously satisfied. Previous studies employing resonant leptogenesis within the scotogenic framework have successfully achieved this goal, but typically at mass scales above 1 TeV [16–19]. In the present work, we aim to lower the mass scale below 1 TeV without resorting to extremely small Yukawa couplings. As a result, the model operates in the strong washout regime, with the decay parameter reaching values as large as 10^5 . This scenario is realized within the framework of tri-resonant leptogenesis [42, 44–46], which requires three nearly degenerate right-handed (RH) neutrinos. Achieving such a spectrum poses a significant challenge from a model-building perspective.

In this work, we implement the scotogenic model within the framework of recently proposed non-holomorphic modular A_4 symmetry [47]. In this setup, it is not necessary to impose an additional Z_2 symmetry, as appropriate modular weight assignments forbid unwanted interactions. Unlike the conventional holomorphic modular symmetry [48], non-holomorphic modular symmetry can be applied to non-supersymmetric (non-SUSY) frameworks. Moreover, it allows for modular forms with negative modular weights, thereby increasing the model-building flexibility while preserving the stringent constraints imposed by modular invariance. In these constructions, Yukawa couplings are not arbitrary

parameters but are determined by modular forms, which are functions of the complex modulus τ . If a generalized CP symmetry [49–53] is imposed consistently with the non-holomorphic modular symmetry [47, 54], the modulus τ becomes the sole complex parameter of the model and thus the only source of CP violation. Since CP violation plays a crucial role in leptogenesis [55], this feature strongly constrains the CP-violating phases and renders the framework highly predictive. There exist previous studies of leptogenesis in holomorphic [56–70] and non-holomorphic [71–74] modular frameworks. As we focus on low-scale leptogenesis, flavor effects become important. Accordingly, we solve the flavor-dependent density matrix equations, which properly account for flavor dynamics in the evolution of the RH neutrino and lepton number densities [75–81]. Within this framework, we demonstrate that three nearly degenerate RH neutrinos can naturally arise when they are assigned to the triplet representation of A_4 . The near degeneracy originates from treating the symmetric contribution to the Majorana mass matrix, arising from the $\mathbf{3} \otimes \mathbf{3}$ decomposition of A_4 , as a small perturbation to the dominant singlet contribution. The singlet term exhibits a $(2, 3)$ symmetry structure, which is broken by the symmetric triplet contribution when treated perturbatively. We note that a scotogenic model based on non-holomorphic modular A_4 symmetry has also been studied in Ref. [82]. However, leptogenesis was not considered in that work, and the modular representations differ from those adopted here. Consequently, our framework leads to distinct phenomenological predictions.

This article is organized as follows. In Section 2, we describe the model and its theoretical framework. In Section 3, we analytically demonstrate how three nearly degenerate RH neutrinos naturally emerge in this setup. In Section 4, we present the numerical analysis and discuss neutrino phenomenology. Section 5 is devoted to the formalism of tri-resonant leptogenesis, where we solve the flavor-dependent density matrix equations to study the evolution of RH neutrino and lepton number densities. Finally, in Section 6, we summarize our results and present our conclusions.

2 Model and Framework

We implement the scotogenic model within a non-holomorphic modular A_4 symmetry framework. The particle content of the model is identical to that of Ma’s original scotogenic model [7]. In addition to the Standard Model field content namely, the left-handed (LH) lepton doublets L_L , the right-handed charged lepton singlets (e_R, μ_R, τ_R) and the Higgs doublet H the model contains three RH neutrinos N_α ($\alpha = 1, 2, 3$) and an inert scalar doublet η .

Instead of imposing a discrete Z_2 symmetry to forbid the tree-level neutrino mass terms, modular weights are employed for this purpose. Fields with odd modular weights effectively behave as Z_2 -odd particles and therefore belong to the dark sector of the model. The assignments of all particles under the Standard Model gauge group and the non-holomorphic modular A_4 symmetry along with their

Fields	L_L	e_R, μ_R, τ_R	N	η	H
$SU(2)_L$	2	1	1	2	2
$U(1)_Y$	-1	-2	-1	-1	1
A_4	3	1, 1', 1''	3	1	1
$-k_I$	-2	2	-1	1	0

Table 1: Charge assignments for various fields under different symmetry groups.

	$Y_1^{(2)}$	$Y_3^{(0)}$	$Y_3^{(2)}$
A_4	1	3	3
k_Y	2	0	2

Table 2: Modular forms, their A_4 representations and modular weights.

corresponding modular weights are summarized in Table 1. In Table 2, we list the modular forms used in the model together with their A_4 representations and modular weights.

The Yukawa Lagrangian for the model is¹

$$\begin{aligned}
\mathcal{L}_Y = & \beta_e [Y_3^{(0)} \bar{L}_L]_1 H e_R + \beta_\mu [Y_3^{(0)} \bar{L}_L]_{1''} H \mu_R + \beta_\tau [Y_3^{(0)} \bar{L}_L]_{1'} H \tau_R \\
& + Y_1^{(2)} \beta_1 [\bar{L}_L N]_1 \eta + Y_3^{(2)} (\beta_2 [\bar{L}_L N]_{3_S} \eta + \beta_3 [\bar{L}_L N]_{3_A} \eta) \\
& + Y_1^{(2)} k_1 [\overline{N^C} N]_1 + Y_3^{(2)} k_2 [\overline{N^C} N]_{3_S} + \text{h.c.}
\end{aligned} \tag{1}$$

where β_l ($l = e, \mu, \tau$), β_i ($i = 1, 2, 3$), and k_i ($i = 1, 2$) are coupling constants. We consider a generalized CP (GCP) symmetry [47, 54], under which all coupling constants are real and the modulus τ is the only complex parameter responsible for CP violation. The A_4 triplet modular forms can be written as $Y_3^{(0)} = (Y_1^0, Y_2^0, Y_3^0)$ and $Y_3^{(2)} = (Y_1^2, Y_2^2, Y_3^2)$.

After applying the rules of A_4 tensor product [83], the relevant Yukawa Lagrangian can be written as

$$\mathcal{L}_Y = Y_c \bar{L}_L H l_R + Y_\eta \bar{L}_L \eta N + M_N \overline{N^C} N + \text{h.c.}, \tag{2}$$

where L_L and l_R denote the LH and RH $SU(2)_L$ lepton doublets and singlets, respectively. The symbol Y_c represents the charged-lepton Yukawa coupling matrix, Y_η denotes the Yukawa coupling matrix involving the RH neutrinos, the inert scalar doublet and the LH lepton doublets and M_N is the bare mass matrix of the RH neutrinos.

¹Here, the notation $[\dots]_r$ indicates that the object inside the brackets transforms as the representation r of the A_4 group.

The charged-lepton Yukawa coupling matrix is non-diagonal and has the following form

$$Y_c = \begin{pmatrix} \beta_e Y_1^0 & \beta_\mu Y_3^0 & \beta_\tau Y_2^0 \\ \beta_e Y_3^0 & \beta_\mu Y_2^0 & \beta_\tau Y_1^0 \\ \beta_e Y_2^0 & \beta_\mu Y_1^0 & \beta_\tau Y_3^0 \end{pmatrix}, \quad (3)$$

and the Yukawa coupling matrix Y_η is of the form

$$Y_\eta = \begin{pmatrix} \beta_1 Y_1^{(2)} + 2Y_1^2 \beta_2 & Y_3^2(-\beta_2 + \beta_3) & Y_2^2(-\beta_2 - \beta_3) \\ Y_3^2(-\beta_2 - \beta_3) & 2Y_2^2 \beta_2 & \beta_1 Y_1^{(2)} + Y_1^2(-\beta_2 + \beta_3) \\ Y_2^2(-\beta_2 + \beta_3) & \beta_1 Y_1^{(2)} + Y_1^2(-\beta_2 - \beta_3) & 2Y_3^2 \beta_2 \end{pmatrix}. \quad (4)$$

The bare mass matrix for the right-handed neutrinos is a complex symmetric matrix of the form

$$M_N = \begin{pmatrix} k_1 Y_1^{(2)} + 2Y_1^2 k_2 & Y_3^2(-k_2) & Y_2^2(-k_2) \\ Y_3^2(-k_2) & 2Y_2^2 k_2 & k_1 Y_1^{(2)} + Y_1^2(-k_2) \\ Y_2^2(-k_2) & k_1 Y_1^{(2)} + Y_1^2(-k_2) & 2Y_3^2 k_2 \end{pmatrix}. \quad (5)$$

This matrix structure exhibits special features for particular choices of the coupling constants, which will be discussed in Section 3. The matrix M_N can be diagonalized as

$$U_R^T M_N U_R = \text{diag}(m_{N_1}, m_{N_2}, m_{N_3}), \quad (6)$$

where U_R is the unitary diagonalizing matrix and m_{N_α} ($\alpha = 1, 2, 3$) are the masses of the three right-handed neutrinos. The scalar potential of the model is

$$\begin{aligned} V(H, \eta) = & -m_H^2 H^\dagger H + m_\eta^2 \eta^\dagger \eta + \lambda_{HH} (H^\dagger H)^2 + \lambda_{\eta\eta} (\eta^\dagger \eta)^2 + \lambda_{H\eta} (H^\dagger H) (\eta^\dagger \eta) \\ & + \lambda'_{H\eta} |H\eta|^2 + \tilde{\lambda} Y^{(-2)} (H\eta)^2 + \text{h.c.} \end{aligned} \quad (7)$$

We define $\lambda \equiv \tilde{\lambda} Y^{(-2)}$, which is complex in general but can be considered real without loss of generality.

The inert scalar doublet η , consisting of a neutral real component η_R , a neutral imaginary component η_I and a charged component η^- with electric charge -1 , can be written as

$$\eta = \begin{pmatrix} \frac{1}{\sqrt{2}}(\eta_R + i\eta_I) \\ \eta^- \end{pmatrix}. \quad (8)$$

After electroweak symmetry breaking, the Standard Model Higgs field acquires a vacuum expectation value $\langle H \rangle = v/\sqrt{2}$ with $v = 246$ GeV, and the masses of the inert scalar bosons can then be written as

$$m_{\eta_R}^2 = m_\eta^2 + \frac{v^2}{2} (\lambda_{H\eta} + \lambda'_{H\eta} + 2\lambda), \quad (9)$$

$$m_{\eta_I}^2 = m_\eta^2 + \frac{v^2}{2} (\lambda_{H\eta} + \lambda'_{H\eta} - 2\lambda), \quad (10)$$

$$m_{\eta^-}^2 = m_\eta^2 + \frac{v^2}{2} \lambda_{H\eta}. \quad (11)$$

The mass-squared difference between the real and imaginary components of the inert scalar doublet, η_R and η_I , respectively, is given by

$$\Delta m^2 = m_{\eta_R}^2 - m_{\eta_I}^2 = 2\lambda v^2. \quad (12)$$

This mass splitting plays a crucial role in the model to satisfy neutrino phenomenology and achieve successful baryogenesis.

The charged lepton mass matrix can be written as

$$M_l = \frac{v}{\sqrt{2}} \begin{pmatrix} \beta_e Y_1^0 & \beta_\mu Y_3^0 & \beta_\tau Y_2^0 \\ \beta_e Y_3^0 & \beta_\mu Y_2^0 & \beta_\tau Y_1^0 \\ \beta_e Y_2^0 & \beta_\mu Y_1^0 & \beta_\tau Y_3^0 \end{pmatrix}. \quad (13)$$

The charged-lepton masses are obtained by diagonalizing the mass matrix M_l with bi-unitary transformations V_L and V_R , *i.e.*,

$$V_L^\dagger M_l V_R = \text{diag}(m_e, m_\mu, m_\tau). \quad (14)$$

Only the matrix V_L has physical effects. Numerically, V_L can be determined by diagonalizing the Hermitian matrix $M_l^H = M_l M_l^\dagger$, which satisfies

$$V_L^\dagger M_l^H V_L = \text{diag}(m_e^2, m_\mu^2, m_\tau^2). \quad (15)$$

Since the charged-lepton masses are known with high precision, we can use their experimental values to determine the three free parameters β_α ($\alpha = e, \mu, \tau$) by means of these three relations

$$\left. \begin{aligned} \text{Tr}[M_l^H] &= |m_e|^2 + |m_\mu|^2 + |m_\tau|^2, \\ \det[M_l^H] &= |m_e|^2 |m_\mu|^2 |m_\tau|^2, \\ (\text{Tr}[M_l^H])^2 - \text{Tr}[M_l^H] &= 2(|m_e|^2 |m_\mu|^2 + |m_\mu|^2 |m_\tau|^2 + |m_e|^2 |m_\tau|^2). \end{aligned} \right\} \quad (16)$$

3 Nearly Degenerate Right-Handed Neutrino Mass Spectrum

The main subject of this paper which is tri-resonant leptogenesis needs nearly three degenerate right-handed neutrinos [42, 44, 45]. This is a great challenge from the model building perspective that we can have such a symmetry originated mass matrix where we can have such scenario. However we have identified that this is possible with existing A_4 non-holomorphic modular symmetry. As, we know that in RH neutrino mass matrix where the RH neutrinos are A_4 triplets, we can have contraction under A_4 tensor product where contribution from the trivial singlet and symmetric part of the $\mathbf{3} \otimes \mathbf{3}$ simultaneously arise in the mass matrix. The resultant matrix, as given in Eqn. (5), can be written in

Parameter	Sampling Range	NH Best Fit	IH Best Fit
$Re[\tau]$	$\pm[0 - 0.5]$	-8.872×10^{-2}	-6.525×10^{-3}
$Im[\tau]$	$[0.8 - 3]$	1.231	1.336
k_1 (GeV)	$[500 - 10^4]$	3.557×10^3	3.467×10^3
k_2 (GeV)	$[10^{-9} - 10^{-2}]$	6.191×10^{-7}	3.007×10^{-7}
β_1	$\pm[10^{-6} - 10^{-3}]$	-5.735×10^{-5}	-1.942×10^{-4}
β_2	$\pm[10^{-6} - 10^{-3}]$	-1.395×10^{-4}	2.037×10^{-4}
β_3	$\pm[10^{-6} - 10^{-3}]$	-1.681×10^{-4}	-2.557×10^{-5}
m_η (GeV)	$[530 - 1500]$	6.492×10^2	6.308×10^2
λ	$[10^{-5} - 10^{-3}]$	7.503×10^{-4}	5.789×10^{-4}

Table 3: The input parameters and their numerical ranges used in the analysis (second column). The best-fit values of free parameters for the normal hierarchy (NH) and inverted hierarchy (IH) are shown in the third and fourth columns, respectively. The minimum chi-square values are $\chi_{\min}^2(\text{NH}) = 0.174$ and $\chi_{\min}^2(\text{IH}) = 14.542$.

the form

$$\tilde{M} = \begin{pmatrix} \tilde{M}_o + kd_1 & kd_4 & kd_5 \\ kd_4 & kd_2 & \tilde{M}_o + kd_6 \\ kd_5 & \tilde{M}_o + kd_6 & kd_3 \end{pmatrix} = \underbrace{\begin{pmatrix} \tilde{M}_o & 0 & 0 \\ 0 & 0 & \tilde{M}_o \\ 0 & \tilde{M}_o & 0 \end{pmatrix}}_{\tilde{M}^{(0)}} + k \underbrace{\begin{pmatrix} d_1 & d_4 & d_5 \\ d_4 & d_2 & d_6 \\ d_5 & d_6 & d_3 \end{pmatrix}}_{\Delta}, \quad (17)$$

where $|k| \ll 1$. When $|k| = 0$, the matrix reduces to $\tilde{M}^{(0)}$. This matrix possesses an exact symmetry in the (2,3) sector and can be diagonalized by the unitary matrix

$$U^{(0)} = \begin{pmatrix} 0 & 1 & 0 \\ i/\sqrt{2} & 0 & 1/\sqrt{2} \\ -i/\sqrt{2} & 0 & 1/\sqrt{2} \end{pmatrix}, \quad (18)$$

such that $(U^{(0)})^T \tilde{M}^{(0)} U^{(0)} = \text{diag}(\tilde{M}_o, \tilde{M}_o, \tilde{M}_o)$, where \tilde{M}_o denotes the eigenvalue of the matrix $\tilde{M}^{(0)}$. Therefore, the spectrum exhibits a threefold degeneracy. We can treat the matrix elements of Δ in the Eqn. (17) as perturbation which can lift this degeneracy by softly breaking the symmetry in (2,3) sector. Therefore, the right-handed neutrino spectrum is naturally nearly-degenerate, without the need for fine-tuning. This feature is a direct consequence of soft breaking of the symmetry in (2,3) sector in a way given in Eqns. (5) or (17) and it provides a natural setting for tri-resonant or quasi-resonant leptogenesis.

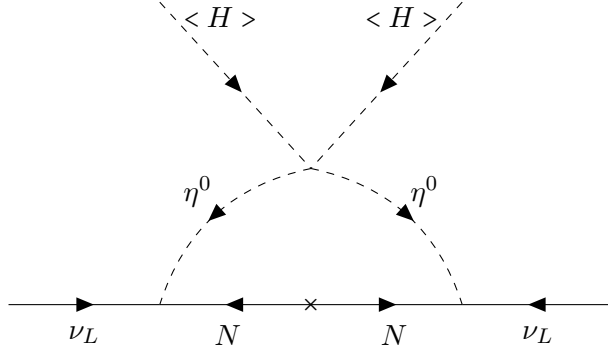


Figure 1: One loop Feynman diagram for neutrino mass generation.

4 Neutrino Phenomenology

The neutrino mass arises from the one-loop diagram (Fig. 1) after spontaneous electroweak symmetry breaking. The resulting neutrino mass matrix is given by

$$M_\nu = \tilde{Y} m^D \tilde{Y}^T, \quad (19)$$

where $m^D = \text{Diag}(m_1^D, m_2^D, m_3^D)$ with

$$m_\alpha^D = \frac{m_{N_\alpha}}{(4\pi)^2} \left[\frac{m_{\eta_R}^2}{m_{\eta_R}^2 - m_{N_\alpha}^2} \ln \left(\frac{m_{\eta_R}^2}{m_{N_\alpha}^2} \right) - \frac{m_{\eta_I}^2}{m_{\eta_I}^2 - m_{N_\alpha}^2} \ln \left(\frac{m_{\eta_I}^2}{m_{N_\alpha}^2} \right) \right], \quad (\alpha = 1, 2, 3), \quad (20)$$

and $\tilde{Y} = Y_\eta U_R$ is the rotated Yukawa coupling in the basis where the right-handed neutrino mass matrix is diagonal. The neutrino mass matrix M_ν can be diagonalized as

$$U_\nu^T M_\nu U_\nu = \text{diag}(m_1, m_2, m_3) \quad (21)$$

where m_i ($i = 1, 2, 3$) are the neutrino masses. The Pontecorvo–Maki–Nakagawa–Sakata (PMNS) mixing matrix is given by $U = V_L^\dagger U_\nu$. Before moving forward let us mention some relations used to calculate the mixing observables in the neutrino sector. Using mixing matrix U , the neutrino mixing angles can be obtained as

$$\sin^2 \theta_{13} = |U_{13}|^2, \quad (22)$$

$$\sin^2 \theta_{23} = \frac{|U_{23}|^2}{1 - |U_{13}|^2}, \quad (23)$$

$$\sin^2 \theta_{12} = \frac{|U_{12}|^2}{1 - |U_{13}|^2}. \quad (24)$$

The Jarlskog CP invariant [84–88], which quantifies the CP violation arising from the Dirac phase δ_{CP} , in the lepton sector is given by

$$J_{CP} = \text{Im}[U_{11}U_{22}U_{12}^*U_{21}^*] = s_{23}c_{23}s_{12}c_{12}s_{13}c_{13}^2 \sin \delta_{CP}, \quad (25)$$

Parameter	NH (best fit)		IH ($\Delta\chi^2 = 5.9$)	
	bfp $\pm 1\sigma$	3σ range	bfp $\pm 1\sigma$	3σ range
$\sin^2 \theta_{12}$	$0.3088^{+0.0067}_{-0.0066}$	$0.2893 \rightarrow 0.3295$	$0.3088^{+0.0067}_{-0.0066}$	$0.2893 \rightarrow 0.3295$
$\theta_{12} [^\circ]$	$33.76^{+0.42}_{-0.41}$	$32.54 \rightarrow 35.03$	$33.76^{+0.42}_{-0.41}$	$32.54 \rightarrow 35.03$
$\sin^2 \theta_{23}$	$0.470^{+0.017}_{-0.014}$	$0.435 \rightarrow 0.584$	$0.550^{+0.013}_{-0.016}$	$0.439 \rightarrow 0.584$
$\theta_{23} [^\circ]$	$43.29^{+0.96}_{-0.79}$	$41.27 \rightarrow 49.86$	$47.90^{+0.73}_{-0.92}$	$41.51 \rightarrow 49.83$
$\sin^2 \theta_{13}$	$0.02248^{+0.00055}_{-0.00059}$	$0.02064 \rightarrow 0.02418$	$0.02262^{+0.00057}_{-0.00056}$	$0.02093 \rightarrow 0.02441$
$\theta_{13} [^\circ]$	$8.62^{+0.11}_{-0.11}$	$8.26 \rightarrow 8.95$	$8.65^{+0.11}_{-0.11}$	$8.32 \rightarrow 8.99$
$\delta_{CP} [^\circ]$	212^{+26}_{-36}	$125 \rightarrow 365$	274^{+22}_{-25}	$203 \rightarrow 335$
$\Delta m_{21}^2 [10^{-5} \text{ eV}^2]$	$7.537^{+0.094}_{-0.100}$	$7.236 \rightarrow 7.823$	$7.537^{+0.094}_{-0.100}$	$7.236 \rightarrow 7.822$
$\Delta m_{3\ell}^2 [10^{-3} \text{ eV}^2]$	$+2.511^{+0.021}_{-0.020}$	$+2.450 \rightarrow +2.576$	$-2.483^{+0.020}_{-0.020}$	$-2.547 \rightarrow -2.421$

Table 4: Neutrino oscillation parameters from NuFIT 6.1 (2025) [94], <http://www.nu-fit.org>. Best-fit values (bfp) with 1σ errors and 3σ ranges are shown. For normal hierarchy (NH) we take $\ell = 1$, while for inverted hierarchy (IH) we take $\ell = 2$.

where s_{ij} (c_{ij}) denotes $\sin \theta_{ij}$ ($\cos \theta_{ij}$). The CP invariants related to the Majorana phases α_{21} and α_{31} [89–92] are

$$I_1 = \text{Im}[U_{11}^* U_{12}] = c_{12} s_{12} c_{13}^2 \sin\left(\frac{\alpha_{21}}{2}\right), \quad (26)$$

$$I_2 = \text{Im}[U_{11}^* U_{13}] = c_{12} s_{13} c_{13} \sin\left(\frac{\alpha_{31}}{2} - \delta_{CP}\right). \quad (27)$$

The effective Majorana mass m_{ee} , which is currently being probed by neutrinoless double beta decay ($0\nu\beta\beta$) experiments and serves as a direct indicator of the Majorana nature of neutrinos, is given by

$$m_{ee} = |(U_{11})^2 m_1 + (U_{12})^2 m_2 + (U_{13})^2 m_3|. \quad (12)$$

An upper bound on the effective Majorana mass, $m_{ee} < (28\text{--}122) \text{ meV}$ at 90% confidence level, has been reported by the KamLAND-Zen experiment [93], where the range reflects uncertainties in nuclear matrix element calculations.

4.1 Numerical Analysis and Results

To study the neutrino phenomenology we have numerically solved the Eqn. (16) and obtained the charged lepton diagonalizing matrix V_L . To obtain the neutrino masses and U_ν we have varied the free parameters in the ranges as shown in the Table 3. It should be noted that our goal is to identify a region of parameter space that can simultaneously satisfy neutrino oscillation data, account for dark matter, and generate the observed baryon asymmetry of the Universe. In this work, we consider the lightest dark sector particle, η_I , with mass m_{η_I} , as the dark matter (DM) candidate. To ensure consistency

Observable	NH Best Fit	IH Best Fit	Observable	NH Best Fit	IH Best Fit
θ_{12} ($^\circ$)	33.81	33.79	I_1	4.358×10^{-1}	-4.034×10^{-4}
θ_{13} ($^\circ$)	8.63	8.68	I_2	9.748×10^{-2}	1.240×10^{-1}
θ_{23} ($^\circ$)	43.16	44.76	$\sum_i m_i$ (meV)	6.144×10^1	1.122×10^2
Δm_{21}^2 (10^{-5}eV^2)	7.523	7.534	m_1 (meV)	2.250	5.027×10^1
Δm_{3l}^2 (10^{-3}eV^2)	2.518	-2.484	m_2 (meV)	8.961	5.101×10^1
δ_{CP} ($^\circ$)	319.127	0.216	m_3 (meV)	5.023×10^1	1.090×10^1
α_{21} ($^\circ$)	149.321	359.898	m_{N_1} (10^2GeV)	7.673566660	9.702325117
α_{31} ($^\circ$)	22.800	179.284	m_{N_2} (10^2GeV)	7.673566667	9.702325120
m_{ee} (meV)	1.135	4.910×10^1	m_{N_3} (10^2GeV)	7.673566682	9.702325128
J_{CP}	-2.214×10^{-2}	1.288×10^{-4}			

Table 5: The neutrino observables evaluated at the best-fit points. The minimum chi-square values are $\chi_{\text{min}}^2(\text{NH}) = 0.174$ and $\chi_{\text{min}}^2(\text{IH}) = 14.542$. For normal hierarchy (NH) we take $\ell = 1$, while for inverted hierarchy (IH) we take $\ell = 2$.

with the experimental bound on the DM relic density, we vary $m_{\eta_I} \simeq m_\eta$ in the range [530–1500] GeV. For appropriate choices of the scalar couplings, this mass range yields the correct relic abundance of dark matter [95–112]. Therefore, we do not discuss the dark matter phenomenology further in this analysis. Since the study of leptogenesis in our model requires small Yukawa couplings in order to suppress washout effects, we exploit the inverse relation between the mass splitting Δm^2 , which is controlled by the coupling λ , and the strength of the Yukawa couplings. Accordingly, we vary λ in the range [10^{-5} – 10^{-3}]. This choice allows us to sufficiently suppress the Yukawa coupling strength while still satisfying the neutrino oscillation data. In order to efficiently scan the parameter space we have used `emcee` package in python [113] and minimized the χ^2 function defined as

$$\chi^2 = \sum_{i=1}^5 \left(\frac{O_i - O_i^{bf}}{\sigma_i} \right)^2, \quad (28)$$

where O_i represents the predicted value of the observable, O_i^{bf} is the corresponding best-fit value and σ_i is the 1σ error from the neutrino oscillation data shown in Table 4. We have considered five observables for our χ^2 function which are the two neutrino mass-squared differences and three neutrino mixing angles. Also, we restrict the parameter space by imposing $|\tau| > 1$.

The results for the normal hierarchy (NH) and inverted hierarchy (IH) of neutrino masses are shown in Fig. 2 and Fig. 3, respectively, and lie within the 3σ range of the data presented in Table 4. The color coding denotes the corresponding χ^2 values, while the red (\times) symbol indicates the global minimum, $\chi_{\text{min}}^2 = 0.174$ for NH and $\chi_{\text{min}}^2 = 14.542$ for IH. The corresponding best-fit parameter values are given in Table 3, and the observables are shown in Table 5.

The allowed regions for the modulus τ in the complex plane are displayed in Fig. 2(a) (Fig. 3(a)) for the

NH (IH). For the NH, the imaginary part is constrained to a very narrow interval, $\text{Im}[\tau] \in [1.20, 1.25]$ while real part lies within $\text{Re}[\tau] \in [\pm 0.05, \pm 0.11]$. In contrast, for the IH, one finds $\text{Im}[\tau] \in [1.328, 1.344]$ and $\text{Re}[\tau] \in [0, \pm 0.04]$. As evident from Fig. 2(b) (3(b)), there is no sharp correlation between $\theta_{12} - \theta_{13}$ in NH (IH). However, in contrast to Fig. 2(c), the $\theta_{13} - \theta_{23}$ correlation is sharply constrained in the IH case (Fig. 3(c)). Moreover, the atmospheric mixing angle θ_{23} is predicted close to maximality $\theta_{23} \in [44.50^\circ, 45.04^\circ]$, in the lower octant. The neutrino mass-squared differences are presented in Fig. 2(d) (Fig. 3(d)) for the NH (IH). The CP invariants and CP-violating phases are shown in Figs. 2(e)–2(g) (Figs. 3(e)–3(g)). In the NH case, we obtain sizable CP violation. In contrast, in the IH case the CP violation is relatively small, particularly from the Dirac phase δ_{CP} and the Majorana phase α_{21} , which has important consequences for baryogenesis. For the NH, the Jarlskog invariant exhibits two localized regions: $J_{CP} \in [0.014, 0.026]$ for $\delta_{CP} \in [25^\circ, 50^\circ]$, and $J_{CP} \in [-0.026, -0.014]$ for $\delta_{CP} \in [310^\circ, 335^\circ]$ (Fig. 2(e)). In contrast, for the IH, J_{CP} is highly suppressed, varying within $J_{CP} \in [0, 0.0008]$ for $\delta_{CP} \in [0^\circ, 1.3^\circ]$, and $J_{CP} \in [-0.0008, 0]$ for $\delta_{CP} \in [358.7^\circ, 360^\circ]$ (Fig. 3(e)). The Majorana CP invariant I_1 in the NH takes values $I_1 \in [0.418, 0.447]$ for $\alpha_{21} \in [141^\circ, 162^\circ]$, and $I_1 \in [-0.447, -0.418]$ for $\alpha_{21} \in [198^\circ, 219^\circ]$ (Fig. 2(f)). For the IH, I_1 remains strongly suppressed, with $I_1 \in [0, 0.00234]$ for $\alpha_{21} \in [0^\circ, 0.6^\circ]$ and $I_1 \in [-0.00234, 0]$ for $\alpha_{21} \in [359.4^\circ, 360^\circ]$. For the second Majorana CP invariant I_2 in the NH, four localized regions are obtained: (i) $I_2 \in [0.078, 0.112]$ for $\alpha_{31} \in [17^\circ, 28^\circ]$; (ii) $I_2 \in [0.063, 0.114]$ for $\alpha_{31} \in [114^\circ, 230^\circ]$; (iii) $I_2 \in [-0.114, -0.063]$ for $\alpha_{31} \in [130^\circ, 246^\circ]$; (iv) $I_2 \in [-0.112, -0.078]$ for $\alpha_{31} \in [332^\circ, 343^\circ]$ (Fig. 2(g)). In the IH case, I_2 is allowed only in a narrow region around $I_2 \in [0.122, 0.127]$ for $\alpha_{31} \in [176^\circ, 180^\circ]$, and $I_2 \in [-0.127, -0.122]$ for $\alpha_{31} \in [180^\circ, 184^\circ]$ (Fig. 3(g)). The predicted ranges for the effective Majorana mass m_{ee} and the sum of neutrino masses ($\sum_i m_i$) are shown in Fig. 2(h) (Fig. 3(h)) for the NH (IH). For the NH case, we have localized region around $m_{ee} \in [0.67, 1.47]$ meV, while the sum of neutrino masses varies within $\sum_i m_i \in [60.51, 62.20]$ meV. In this figure, the horizontal line represents the projected sensitivity of the nEXO [114] neutrinoless double beta ($0\nu\beta\beta$) decay experiment, while the vertical lines denote the cosmological upper bounds on the sum of neutrino masses from DESI+BAO ($\sum_i m_i \leq 72$ meV) [115] and Planck ($\sum_i m_i \leq 120$ meV) [116]. As can be seen, for the NH, m_{ee} lies well below the nEXO sensitivity, whereas $\sum_i m_i \simeq 60.51\text{--}62.20$ meV is comfortably below the current cosmological upper limits (Fig. 2(h)). In contrast, for the IH, the effective Majorana mass lies in the range $m_{ee} \in [48.43, 49.75]$ meV, while the sum of neutrino masses spans $\sum_i m_i \in [110.52, 113.72]$ meV (Fig. 3(h)). In this figure, the light blue band indicates the upper bound on m_{ee} obtained by KamLAND-Zen, namely $m_{ee} < (28\text{--}122)$ meV at 90% C.L [93]. In this case, m_{ee} falls within the sensitivity reach of upcoming $0\nu\beta\beta$ experiments, while $\sum_i m_i$ is close to the Planck limit but significantly above the DESI+BAO upper bound. Given the KamLAND-Zen constraint, the inverted hierarchy scenario may be strongly constrained or potentially excluded by future experimental data. Similarly, forthcoming cosmological observations, particularly from Planck, are expected to further constrain $\sum_i m_i$ (Fig. 3(h)). Finally, we briefly address lepton flavor violation (LFV). The Yukawa couplings in our framework are naturally small, leading to LFV rates well below

existing experimental limits [117]. Consequently, LFV constraints do not impose additional restrictions on the parameter space considered here, and we therefore omit a detailed discussion.

5 Tri-Resonant Leptogenesis

In this section, we discuss *tri-resonant leptogenesis*. As outlined in the introduction, resonant leptogenesis is one of the viable mechanisms for generating the observed baryon asymmetry of the Universe at energy scales below 1 TeV within the scotogenic model. In this framework, accommodating neutrino oscillation data typically requires relatively large Yukawa couplings. However, successful baryogenesis demands smaller Yukawa couplings in order to suppress washout processes. Reducing the Yukawa couplings generally suppresses the CP asymmetry, thereby making baryogenesis difficult to achieve. This situation changes significantly in the presence of nearly degenerate right-handed (RH) neutrinos. When the mass splitting between two RH neutrinos, defined as $\delta_{ij} = |m_{N_i} - m_{N_j}|$, becomes comparable to half of the decay width of the decaying particle, $\Gamma_{i,j}$, *i.e.*,

$$\delta_{ij} \simeq \frac{\Gamma_{i,j}}{2}, \quad (29)$$

the CP asymmetry undergoes resonant enhancement [41–43]. As a result, large CP asymmetries can be generated even for relatively small Yukawa couplings, allowing for successful baryogenesis.

In our framework, we have three nearly degenerate RH neutrinos with a mass ordering $m_{N_1} \lesssim m_{N_2} \lesssim m_{N_3}$. In this case, the enhancement is further amplified since all three RH neutrinos can contribute to the generation of the lepton asymmetry through their decays. Moreover, as we study leptogenesis at low energy scales (below 1 TeV), flavor effects become relevant and can further enhance the CP asymmetry. Consequently, we anticipate that successful baryogenesis can be achieved in our model even in the deep strong-washout regime, as will be demonstrated later in this section.

In the tri-resonant leptogenesis scenario, a maximally enhanced CP asymmetry is generated due to the mixing among all three right-handed singlet neutrinos [42, 44, 45]. The full set of resonant effects contributing to the CP asymmetry arising from this mixing can be systematically captured through the resummed effective Yukawa couplings $(Y_+)_{l\alpha}$ and $(Y_-)_{l\alpha}$. The effective Yukawa coupling $(Y_+)_{l\alpha}$ is associated to the $L\eta N$ interaction, which can be written as

$$(Y_+)_{l\alpha} = Y_{l\alpha} + iV_{l\alpha} - i \sum_{\beta,\gamma=1}^3 |\epsilon_{\alpha\beta\gamma}| Y_{l\beta} \times \frac{m_{N_\alpha} (M_{\alpha\alpha\beta} + M_{\beta\beta\alpha}) - iR_{\alpha\gamma} [M_{\alpha\gamma\beta} (M_{\alpha\alpha\gamma} + M_{\gamma\gamma\alpha}) + M_{\beta\beta\gamma} (M_{\alpha\gamma\alpha} + M_{\gamma\alpha\gamma})]}{m_{N_\alpha}^2 - m_{N_\beta}^2 + 2im_{N_\alpha}^2 A_{\beta\beta} + 2i \text{Im} R_{\alpha\gamma} (m_{N_\alpha}^2 |A_{\beta\gamma}|^2 + m_{N_\beta} m_{N_\gamma} \text{Re} A_{\beta\gamma}^2)}, \quad (30)$$

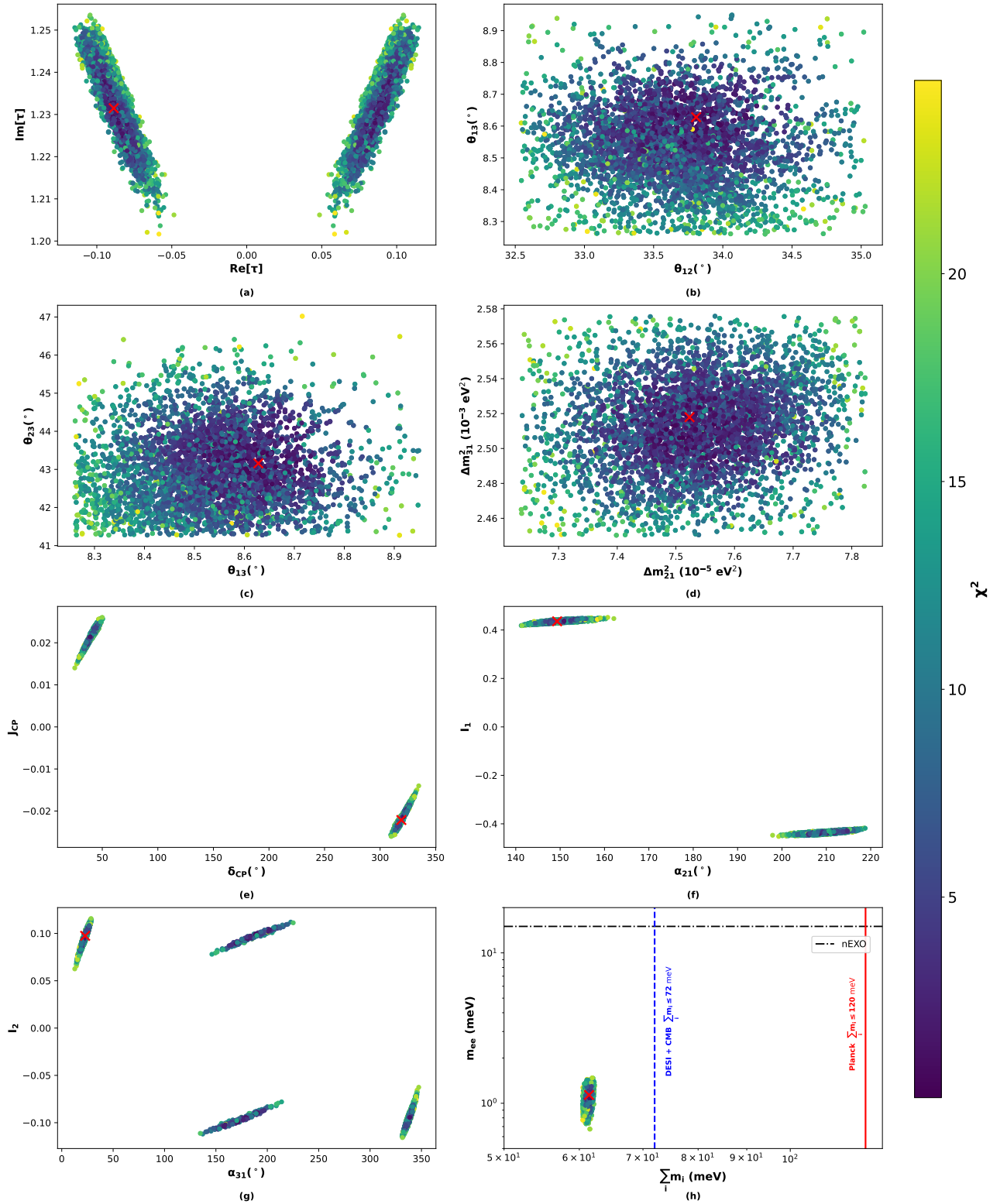


Figure 2: Model predictions for NH with neutrino oscillation parameters within the 3σ range of NuFIT 6.1 (Table 4). Point colors indicate the corresponding χ^2 values, and the red cross (\times) symbol denotes the best-fit point with $\chi^2_{\min} = 0.174$. The horizontal line in Fig. 2(h) represents the $0\nu\beta\beta$ experimental sensitivity, and the vertical lines indicate cosmological upper bounds on $\sum_i m_i$.

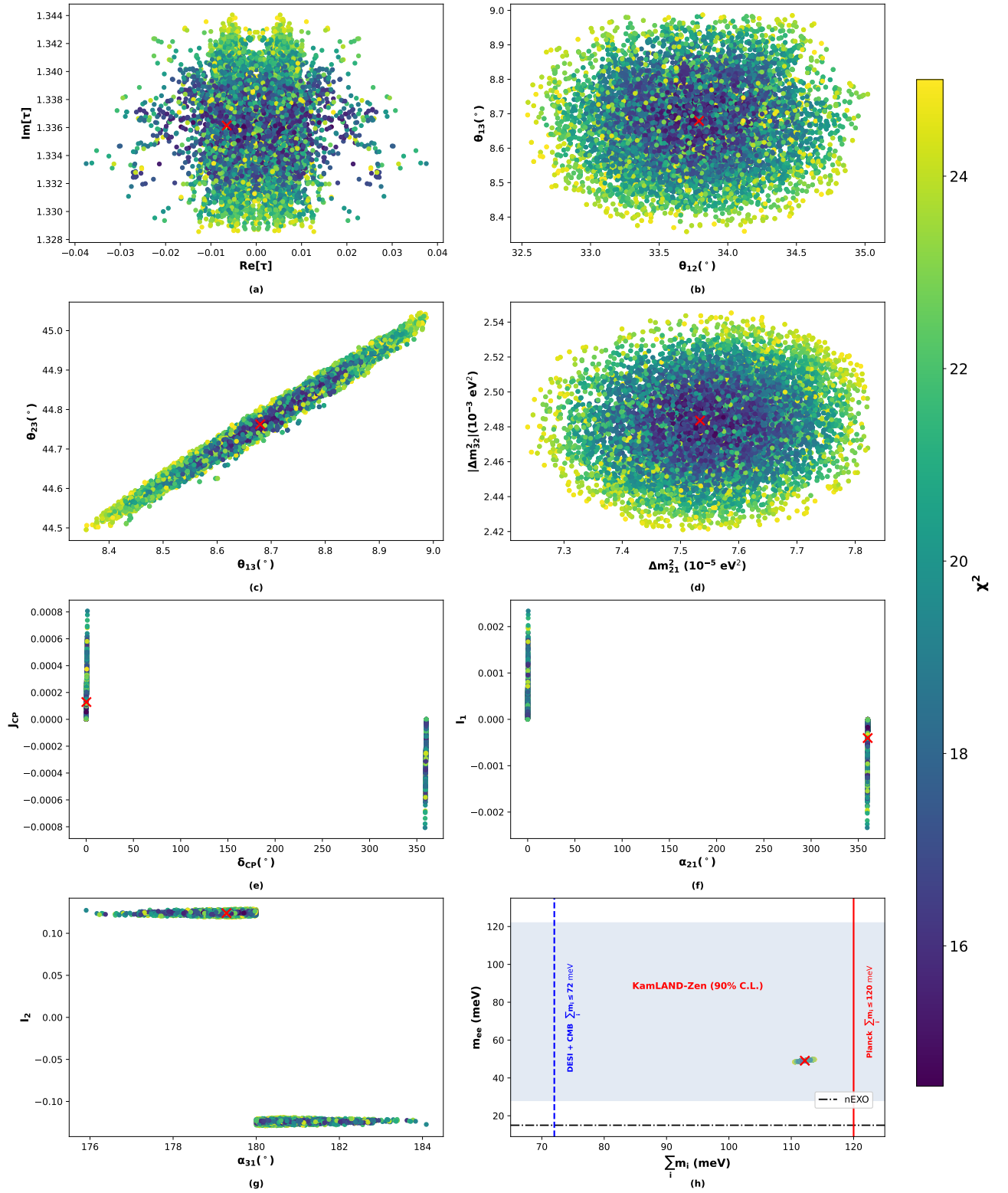


Figure 3: Model predictions for IH with neutrino oscillation parameters within the 3σ range of NuFIT 6.1 (Table 4). Point colors indicate the corresponding χ^2 values, and the red cross (X) symbol denotes the best-fit point with $\chi^2_{\min} = 14.542$. The light blue shaded region in Fig. 3(h) shows the KamLAND-Zen upper bound, the horizontal line represents the $0\nu\beta\beta$ experimental sensitivity, and the vertical lines indicate cosmological upper bounds on $\sum_i m_i$.

where $Y = V_L^\dagger Y_\eta U_R$, $\epsilon_{\alpha\beta\gamma}$ is the anti-symmetric Levi-Civita symbol, $M_{\alpha\beta\gamma} \equiv m_{N_\alpha} A_{\beta\gamma}$ and

$$A_{\alpha\beta} = \sum_{l=1}^3 \frac{Y_{l\alpha} Y_{l\beta}^*}{16\pi} = \frac{(Y^\dagger Y)_{\alpha\beta}^*}{16\pi}, \quad (31)$$

$$V_{l\alpha} = \sum_{k=1}^3 \sum_{\gamma \neq \alpha} \frac{Y_{k\alpha}^* Y_{k\gamma} Y_{l\gamma}}{16\pi} f\left(\frac{m_{N_\gamma}^2}{m_{N_\alpha}^2}\right), \quad (32)$$

$$R_{\alpha\beta} \equiv \frac{m_{N_\alpha}^2}{m_{N_\alpha}^2 - m_{N_\beta}^2 + 2im_{N_\alpha}^2 A_{\beta\beta}}. \quad (33)$$

Here, $A_{\alpha\beta}$ and $V_{l\alpha}$ represent the absorptive transition amplitudes arising from the propagator and vertex contributions, respectively. The quantity $f(x) = \sqrt{x} \left[1 - (1+x) \ln\left(\frac{1+x}{x}\right) \right]$ denotes the Fukugita–Yanagida one-loop function [35].

The effective Yukawa coupling $(Y_-)_{l\alpha}$ associated to $\bar{L}\bar{\eta}N$ interaction can be obtained from Eqn. (30) by replacing $Y_{l\alpha}$ with $Y_{l\alpha}^*$. The radiatively corrected partial decay widths in terms of these effective Yukawa couplings can be written as

$$\Gamma_\alpha = \sum_{l=e,\mu,\tau} \Gamma(N_\alpha \rightarrow L_l + \eta) = \frac{m_{N_\alpha}}{16\pi} (Y_+^\dagger Y_+)_{\alpha\alpha} \left(1 - \frac{m_\eta^2}{m_{N_\alpha}^2}\right)^2, \quad (34)$$

$$\bar{\Gamma}_\alpha = \sum_{l=e,\mu,\tau} \Gamma(N_\alpha \rightarrow \bar{L}_l + \bar{\eta}) = \frac{m_{N_\alpha}}{16\pi} (Y_-^\dagger Y_-)_{\alpha\alpha} \left(1 - \frac{m_\eta^2}{m_{N_\alpha}^2}\right)^2, \quad (35)$$

and we can write total decay width as

$$\Gamma_\alpha^T = \Gamma_\alpha + \bar{\Gamma}_\alpha = \frac{m_{N_\alpha}}{16\pi} \left[(Y_+^\dagger Y_+)_{\alpha\alpha} + (Y_-^\dagger Y_-)_{\alpha\alpha} \right] \left(1 - \frac{m_\eta^2}{m_{N_\alpha}^2}\right)^2. \quad (36)$$

The CP-asymmetry matrix element $\varepsilon_{ll'}^\alpha$ can be written as the ratio of the difference of these partial decay widths to the total decay width, and it determines the asymmetry generated in each N_α decay as

$$\varepsilon_{ll'}^\alpha = \frac{\bar{P}_{ll'}^\alpha \bar{\Gamma}_\alpha - P_{ll'}^\alpha \Gamma_\alpha}{\Gamma_\alpha^T}, \quad (37)$$

The two projectors $P_{ll'}^\alpha$ and $\bar{P}_{ll'}^\alpha$ in the above expression are given by

$$P_{ll'}^\alpha = C_{\alpha l} C_{\alpha l'}^*, \quad \bar{P}_{ll'}^\alpha = \bar{C}_{\alpha l} \bar{C}_{\alpha l'}^*, \quad (38)$$

with amplitudes

$$C_{\alpha l} = \frac{(Y_+)_{l\alpha}}{\sqrt{(Y_+^\dagger Y_+)_{\alpha\alpha}}}, \quad \bar{C}_{\alpha l} = \frac{(Y_-)_{l\alpha}}{\sqrt{(Y_-^\dagger Y_-)_{\alpha\alpha}}}. \quad (39)$$

At tree level, these amplitudes becomes

$$C_{\alpha l}^0 = \frac{Y_{l\alpha}}{\sqrt{(Y^\dagger Y)_{\alpha\alpha}}}. \quad (40)$$

In the CP asymmetry matrix, each diagonal entry corresponds to the flavored CP asymmetry $\varepsilon_{ll}^\alpha = \varepsilon_{\alpha l}$, which is real. In contrast, the off-diagonal entries satisfy $\varepsilon_{ll'}^\alpha = (\varepsilon_{l'l}^\alpha)^*$ and can, in general, be complex.

The total CP asymmetry ε_α in the decay of N_α is obtained by taking the trace of the CP asymmetry matrix, i.e., $\varepsilon_\alpha = \sum_l \varepsilon_{ll}^\alpha$. The total CP asymmetry then can be written as $\varepsilon_T = \sum_\alpha \varepsilon_\alpha$.

To determine the evolution of the right-handed (RH) neutrino number density n_{N_α} and the lepton asymmetry number density $n_{\ell\ell'}$, generated in each flavor through the decays of N_α , we must solve evolution equations that explicitly account for flavor effects. The evolution is studied as a function of the dimensionless parameter $z \equiv m_{N_1}/T$, where m_{N_1} is the mass of the lightest RH neutrino and T is the temperature of the Universe. For this purpose, we employ density matrix equations, which are particularly well suited for tracking flavor dynamics and can be written as [46, 75–81]

$$\begin{aligned}
\frac{dn_{N_\alpha}}{dz} &= -D_\alpha (n_{N_\alpha} - n_{N_\alpha}^{\text{eq}}), \\
\frac{dn_{ee}}{dz} &= \sum_{\alpha=1}^3 \left\{ \varepsilon_{ee}^\alpha D_\alpha (n_{N_\alpha} - n_{N_\alpha}^{\text{eq}}) - W_\alpha \left[|C_{\alpha e}^0|^2 n_{ee} + \text{Re} \left[C_{\alpha e}^{0*} (C_{\alpha\mu}^0 n_{\mu e}^* + C_{\alpha\tau}^0 n_{\tau e}^*) \right] \right] \right\}, \\
\frac{dn_{\mu\mu}}{dz} &= \sum_{\alpha=1}^3 \left\{ \varepsilon_{\mu\mu}^\alpha D_\alpha (n_{N_\alpha} - n_{N_\alpha}^{\text{eq}}) - W_\alpha \left[|C_{\alpha\mu}^0|^2 n_{\mu\mu} + \text{Re} \left[C_{\alpha\mu}^{0*} (C_{\alpha e}^0 n_{\mu e} + C_{\alpha\tau}^0 n_{\tau\mu}^*) \right] \right] \right\}, \\
\frac{dn_{\tau\tau}}{dz} &= \sum_{\alpha=1}^3 \left\{ \varepsilon_{\tau\tau}^\alpha D_\alpha (n_{N_\alpha} - n_{N_\alpha}^{\text{eq}}) - W_\alpha \left[|C_{\alpha\tau}^0|^2 n_{\tau\tau} + \text{Re} \left[C_{\alpha\tau}^{0*} (C_{\alpha e}^0 n_{\tau e} + C_{\alpha\mu}^0 n_{\tau\mu}) \right] \right] \right\}, \\
\frac{dn_{\tau\mu}}{dz} &= \sum_{\alpha=1}^3 \left\{ \varepsilon_{\tau\mu}^\alpha D_\alpha (n_{N_\alpha} - n_{N_\alpha}^{\text{eq}}) - \frac{1}{2} W_\alpha \left[n_{\tau\mu} (|C_{\alpha\tau}^0|^2 + |C_{\alpha\mu}^0|^2) + C_{\alpha\mu}^{0*} C_{\alpha\tau}^0 (n_{\tau\tau} + n_{\mu\mu}) \right. \right. \\
&\quad \left. \left. + C_{\alpha e}^{0*} C_{\alpha\tau}^0 n_{\mu e}^* + C_{\alpha\mu}^{0*} C_{\alpha e}^0 n_{\tau e} \right] \right\} - \left[\text{Im}(\Lambda_\tau) + \text{Im}(\Lambda_\mu) \right] \frac{n_{\tau\mu}}{Hz}, \\
\frac{dn_{\tau e}}{dz} &= \sum_{\alpha=1}^3 \left\{ \varepsilon_{\tau e}^\alpha D_\alpha (n_{N_\alpha} - n_{N_\alpha}^{\text{eq}}) - \frac{1}{2} W_\alpha \left[n_{\tau e} (|C_{\alpha e}^0|^2 + |C_{\alpha\tau}^0|^2) + C_{\alpha e}^{0*} C_{\alpha\tau}^0 (n_{ee} + n_{\tau\tau}) \right. \right. \\
&\quad \left. \left. + C_{\alpha\mu}^{0*} C_{\alpha\tau}^0 n_{\mu e} + C_{\alpha e}^{0*} C_{\alpha\mu}^0 n_{\tau\mu} \right] \right\} - \text{Im}(\Lambda_\tau) \frac{n_{\tau e}}{Hz}, \\
\frac{dn_{\mu e}}{dz} &= \sum_{\alpha=1}^3 \left\{ \varepsilon_{\mu e}^\alpha D_\alpha (n_{N_\alpha} - n_{N_\alpha}^{\text{eq}}) - \frac{1}{2} W_\alpha \left[n_{\mu e} (|C_{\alpha e}^0|^2 + |C_{\alpha\mu}^0|^2) + C_{\alpha e}^{0*} C_{\alpha\mu}^0 (n_{ee} + n_{\mu\mu}) \right. \right. \\
&\quad \left. \left. + C_{\alpha e}^{0*} C_{\alpha\tau}^0 n_{\tau\mu}^* + C_{\alpha\tau}^{0*} C_{\alpha\mu}^0 n_{\tau e} \right] \right\} - \text{Im}(\Lambda_\mu) \frac{n_{\mu e}}{Hz}. \tag{41}
\end{aligned}$$

In these equations $n_{N_\alpha}^{\text{eq}}$ is the equilibrium number density of the RH neutrino N_α ($\alpha = 1, 2, 3$) and symbol D_α and W_α denote the decays and washouts² due to inverse decay, respectively, in thermal plasma and can be written as

$$D_\alpha(z) = K_\alpha x_\alpha z \frac{\mathcal{K}_1(z_\alpha)}{\mathcal{K}_2(z_\alpha)}, \tag{42}$$

$$W_\alpha(z) = \frac{1}{4} K_\alpha \sqrt{x_\alpha} z_\alpha^3 \mathcal{K}_1(z_\alpha). \tag{43}$$

In the above expressions, $K_\alpha = \Gamma_\alpha^T/H(z=1)$ is the decay parameter, where the Hubble expansion rate is given by

$$H(z) = \sqrt{\frac{4\pi^3 g_\star}{45}} \frac{m_{N_1}^2}{z^2 M_{\text{Pl}}}. \tag{44}$$

²As, we are in strong-washout region so we can safely neglect the $\Delta L = 1$ and $\Delta L = 2$ scattering processes [10, 36].

Here $g_* = 116$ denotes the effective number of relativistic degrees of freedom in the early Universe, and $M_{\text{Pl}} = 1.22 \times 10^{19}$ GeV is the Planck mass. The symbols \mathcal{K}_1 and \mathcal{K}_2 denote the modified Bessel functions of the second kind and we define $x_\alpha \equiv m_{N_\alpha}^2/m_{N_1}^2$, $z_\alpha \equiv z\sqrt{x_\alpha}$. The symbol Λ_l in Eq. (41) denotes the self-energy associated with the charged lepton of flavor l . Its imaginary part is related to the Yukawa coupling y_l of the corresponding charged lepton and temperature T , and is approximately given by [79]

$$\text{Im}(\Lambda_l) \simeq 8 \times 10^{-3} y_l^2 T. \quad (45)$$

The lepton density matrix $n_{ll'}$ is a 3×3 matrix whose diagonal elements n_{ll} are real, while the off-diagonal elements are, in general, complex. The total lepton asymmetry can be obtained from this matrix by taking its trace,

$$n_{B-L}(z) = \sum_{l=e,\mu,\tau} n_{ll}(z). \quad (46)$$

This asymmetry is subsequently partially converted into a baryon asymmetry through $B-L$ conserving sphaleron transitions. The final baryon asymmetry can be written as

$$\eta_B = 0.012 n_{B-L}(z_{\text{sph}}), \quad (47)$$

where $z_{\text{sph}} = m_{N_1}/T_{\text{sph}}$, and $T_{\text{sph}} = 131.7$ GeV is the sphaleron freeze-out temperature [118]. This result is then compared with the experimentally observed value of the baryon asymmetry, $\eta_B = (6.12 \pm 0.04) \times 10^{-10}$, as inferred from measurements of the cosmic microwave background (CMB) [116].

In addition to the study of successful baryogenesis at low energy, in our model, we also aim to investigate the relationship between the required mass degeneracy needed to obtain the correct baryon asymmetry and the strong washout regime. For this purpose, we consider two types of benchmark points BP1 and BP2 for each mass hierarchy (*i.e.*, NH and IH), classified according to the strength of the washout of the generated asymmetry. The BP1 and BP2 corresponds to low and high decay parameter strength relative to each other, respectively. The benchmark points, along with the corresponding decay parameters (K_α), are presented in Table 6. The results obtained are shown in Fig. 4 (Fig. 5) for NH (IH), where first and second row corresponds to BP1 and BP2, respectively. We consider zero initial abundances for both right-handed neutrinos and leptons. In the case of normal hierarchy (NH), BP1 corresponds to a right-handed (RH) neutrino mass of approximately 537 GeV while for BP2 the mass is around 592 GeV. Figure 4(a) (Fig. 4(c)) shows the evolution of the number densities of each RH neutrino species along with their corresponding equilibrium values for BP1 (BP2). The decay parameter is inversely related to z_{eq} [40], defined as the value of z at which $n_{N_\alpha}(z_{\text{eq}}) = n_{N_\alpha}^{\text{eq}}(z_{\text{eq}})$. This behavior is clearly visible in the figures, a larger decay parameter corresponds to a smaller value of z_{eq} for the corresponding RH neutrino species. For $z > z_{\text{eq}}$, the RH neutrino number densities closely follow their equilibrium values, indicating that the system lies in the strong washout regime. From Fig. 4(b) (Fig. 4(d)) for BP1 (BP2), we observe that as n_{N_α} in Fig. 4(a) (Fig. 4(c)) approaches its equilibrium value, the lepton asymmetry in different flavors, $|n_{\ell\ell}|$, also approaches its maximum value. Subsequently, the lepton asymmetry is washed out and begins to decrease. In the region below the sphaleron freeze-out point z_{sph} , indicated

Quantity	BP1 (NH)	BP2 (NH)	BP1 (IH)	BP2 (IH)
$Re[\tau]$	1.088×10^{-1}	-7.598×10^{-2}	-6.586×10^{-3}	-9.428×10^{-3}
$Im[\tau]$	1.247	1.214	1.331	1.333
k_1 (10^3 GeV)	2.366	2.922	2.064	2.005
k_2 (GeV)	2.987×10^{-4}	7.015×10^{-7}	6.626×10^{-6}	1.471×10^{-6}
β_1	-3.868×10^{-5}	-7.487×10^{-5}	-1.985×10^{-4}	-2.069×10^{-4}
β_2	-1.282×10^{-4}	-1.437×10^{-4}	2.082×10^{-4}	2.170×10^{-4}
β_3	-1.566×10^{-4}	-1.723×10^{-4}	-2.665×10^{-5}	-2.752×10^{-5}
m_η (10^2 GeV)	5.313	5.314	5.665	5.441
λ	7.626×10^{-4}	5.762×10^{-4}	5.495×10^{-4}	4.806×10^{-4}
m_{N_1} (10^2 GeV)	5.372075	5.92791349	5.7227086	5.57781227
m_{N_2} (10^2 GeV)	5.372078	5.92791350	5.7227087	5.57781228
m_{N_3} (10^2 GeV)	5.372085	5.92791352	5.7227089	5.57781232
$ \varepsilon_T $	3.438×10^{-4}	6.723×10^{-2}	2.412×10^{-4}	1.471×10^{-3}
K_1	1.211×10^3	1.098×10^5	2.613×10^3	1.696×10^4
K_2	1.249×10^3	1.146×10^5	6.172×10^2	4.038×10^3
K_3	1.838×10^3	1.765×10^5	2.653×10^3	1.722×10^4
δ_{12}/m_{N_1}	5.940×10^{-7}	1.407×10^{-9}	1.046×10^{-8}	2.371×10^{-9}
δ_{23}/m_{N_2}	1.408×10^{-6}	2.945×10^{-9}	3.008×10^{-8}	6.855×10^{-9}
δ_{13}/m_{N_1}	2.002×10^{-6}	4.351×10^{-9}	4.054×10^{-8}	9.226×10^{-9}
η_B	6.12×10^{-10}	6.12×10^{-10}	6.12×10^{-10}	6.12×10^{-10}
χ^2	15.593	9.792	20.203	17.665

Table 6: The benchmark points (BP1 and BP2) for both NH and IH considered in the numerical analysis of the density matrix equations.

by the red vertical dot-dashed line, the generated lepton asymmetry can be partially converted into the baryon asymmetry of the Universe. The final baryon asymmetry is therefore fixed at $z = z_{\text{sph}}$, beyond which sphaleron processes become ineffective and no further conversion is possible. This final value corresponds to the baryon asymmetry observed today. As can be seen from the Figs. 4(b) and 4(d), where evolution of baryon asymmetry $|\eta_B|$ is shown in black dot-dashed line, we successfully obtain the observed baryon asymmetry, $\eta_B = 6.12 \times 10^{-10}$, for both benchmark points at $z = z_{\text{sph}}$.

As evident from the data in Table 6, the required degeneracy δ_{ij}/m_{N_i} among RH neutrino masses for BP1 is of order $\mathcal{O}(10^{-7} - 10^{-6})$, whereas for BP2 it is $\mathcal{O}(10^{-9})$. This difference arises because BP2 lies deep in the strong washout regime. Consequently, achieving the correct baryon asymmetry requires a larger total CP asymmetry ε_T (see Table 6), which in turn necessitates being closer to the resonant condition. It is also noteworthy that, despite having Yukawa couplings of order $\mathcal{O}(10^{-5} - 10^{-4})$, the

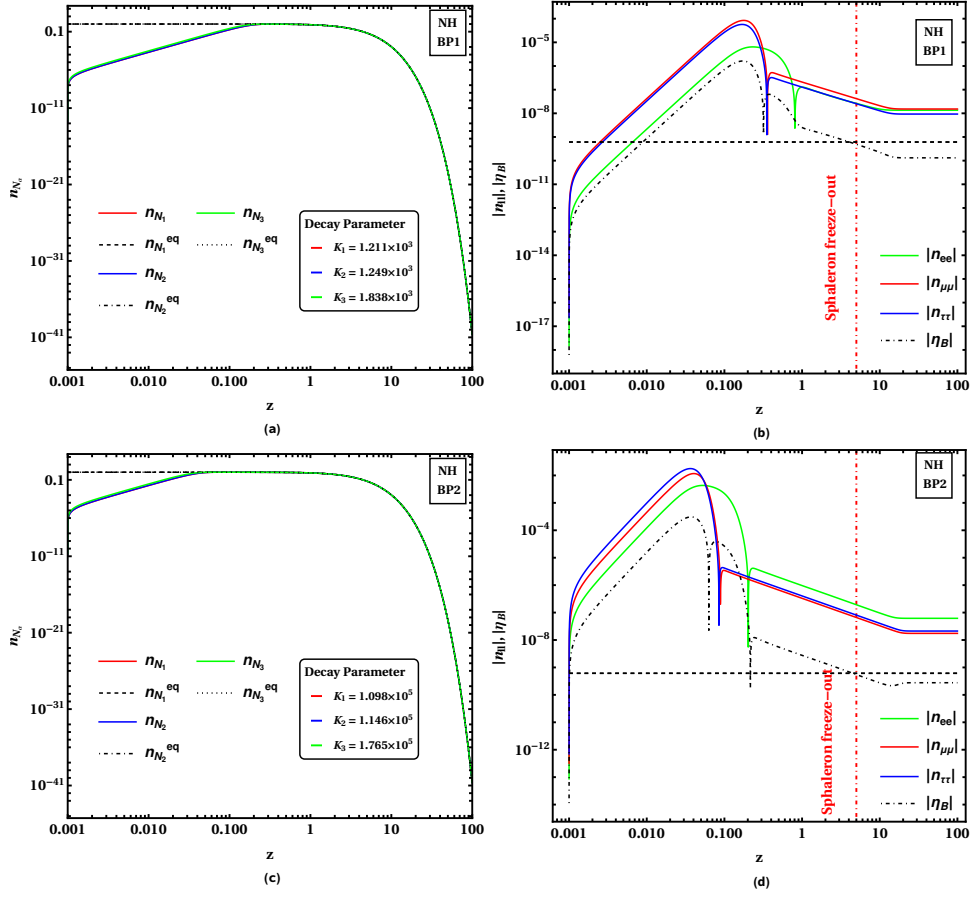


Figure 4: Evolution of the number density of each right-handed neutrino in Fig. 4(a) (4(c)) and evolution of the number density of each lepton flavor together with the baryon asymmetry in Fig. 4(b) (4(d)) as a function of z for BP1 (BP2) in the normal hierarchy (NH) case. The horizontal dashed black line and the vertical dot-dashed red line in Fig. 4(b) and Fig. 4(d) indicate the experimentally observed value of the baryon asymmetry and the sphaleron freeze-out, respectively. Zero initial abundance is assumed for all particle species.

correct baryon asymmetry can still be obtained for RH neutrino masses as low as 537 GeV. We also noted that in order to have observed baryon asymmetry value we need not to go very near the resonance and thus fine tuning is not required.

In the case of inverted hierarchy (IH), BP1 corresponds to RH neutrino mass of 572 GeV, while BP2 corresponds to a mass of 557 GeV. Figure 5(a) (Fig. 5(c)) shows the evolution of RH neutrino number densities for BP1 (BP2), while Fig. 5(b) (Fig. 5(d)) shows the evolution of the generated lepton asymmetry and the final baryon asymmetry for BP1 (BP2). The qualitative behavior in the IH case is similar to that discussed for NH and is therefore not repeated here. However, it is important to note that for BP1 in IH case, the degeneracy δ_{ij}/m_{N_i} among RH neutrinos required for successful baryogenesis is of the order $\mathcal{O}(10^{-8})$ (see Table 6). This is because the total CP asymmetry ε_T value cannot be very large due to the small CP violation, as evident from the values of the CP invariants and CP phases discussed in the previous section. In fact, only the Majorana phase α_{23} deviates significantly from trivial values. As a result, one must move closer to the resonance to obtain the correct baryon asymmetry. For BP2

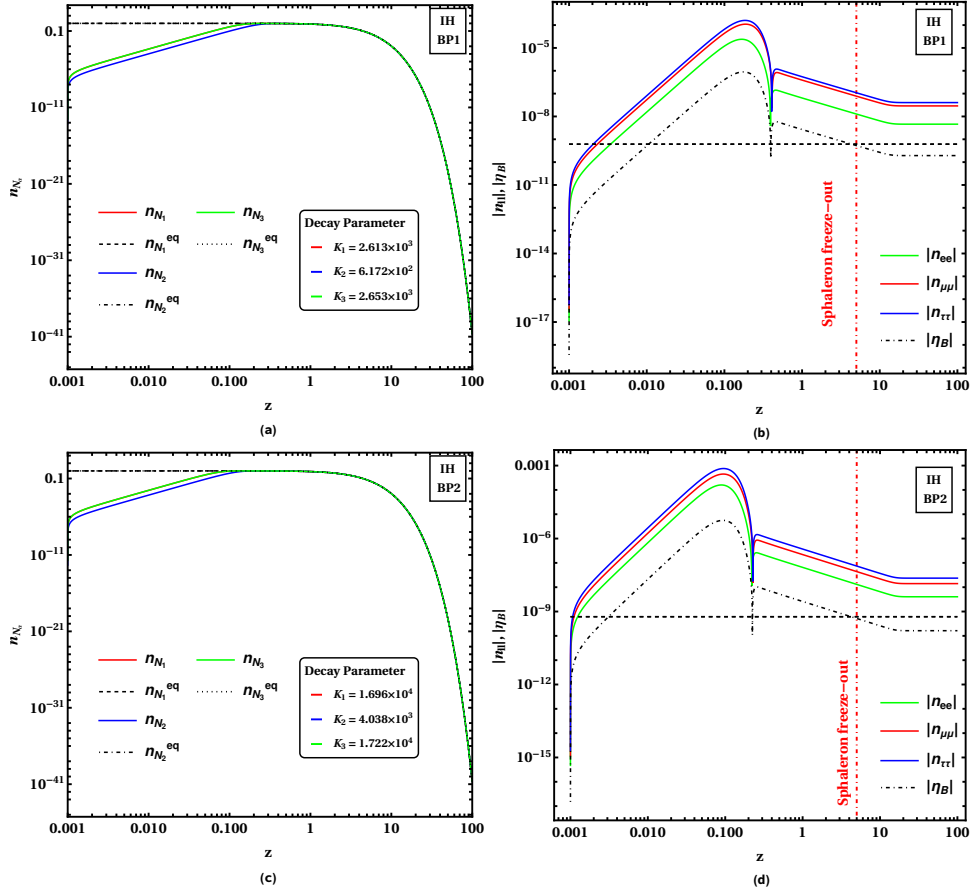


Figure 5: Evolution of the number density of each right-handed neutrino in Fig. 5(a) (5(c)) and evolution of the number density of each lepton flavor together with the baryon asymmetry in Fig. 5(b) (5(d)) as a function of z for BP1 (BP2) in the normal hierarchy (NH) case. The horizontal dashed black line and the vertical dot-dashed red line in Fig. 5(b) and Fig. 5(d) indicate the experimentally observed value of the baryon asymmetry and the sphaleron freeze-out, respectively. Zero initial abundance is assumed for all particle species.

in the IH case, the required degeneracy is of order $\mathcal{O}(10^{-9})$. In this case also we have successfully obtained the baryon asymmetry value, $\eta_B = 6.12 \times 10^{-10}$ for both benchmark points at $z = z_{\text{sph}}$. We also noted that, it is very difficult to obtain the experimentally observed baryon asymmetry in IH case if we consider point with higher decay parameter even if we go very close to resonance.

6 Conclusions

In this work, we have successfully implemented the scotogenic model within the framework of non-holomorphic A_4 modular symmetry. We have demonstrated that this framework naturally accommodates three nearly degenerate right-handed (RH) neutrinos. This feature arises when the symmetric contribution to the Majorana mass matrix, originating from the $\mathbf{3} \otimes \mathbf{3}$ decomposition of the A_4 group representation is treated as a small perturbation to the dominant contribution from the singlet component of the same product. We have identified regions of parameter space that are consistent with

current neutrino oscillation data. In this model, the complex modulus τ is the only complex parameter and therefore serves as the sole source of CP violation. For both normal (NH) and inverted (IH) mass hierarchies, τ is restricted to a very narrow region in the complex plane making the model highly predictive and leading to testable consequences. In the NH case, we have sizable CP violation. While it is relatively small with only Majorana phase α_{23} taking non-trivial values in IH. Additional hierarchy-dependent predictions arise for the atmospheric mixing angle θ_{23} , the effective Majorana mass m_{ee} , and the sum of neutrino masses $\sum_i m_i$. For NH, the atmospheric mixing angle θ_{23} is not strongly constrained. The effective Majorana mass m_{ee} lies below the projected sensitivity of upcoming neutrinoless double beta decay ($0\nu\beta\beta$) experiments, while the sum of neutrino masses $\sum_i m_i$ remains safely below current cosmological upper bounds. In contrast, for the IH case, θ_{23} is predicted to be close to maximal mixing, lying in the lower octant within the range $\theta_{23} \in [44.50^\circ, 45.04^\circ]$. The predicted values of m_{ee} fall within the sensitivity reach of KamLAND-Zen and future $0\nu\beta\beta$ experiments. Moreover, $\sum_i m_i$ lies close to the present upper limit from Planck observations, making it testable by forthcoming cosmological measurements. Furthermore, we have studied tri-resonant leptogenesis within this model and successfully generated the observed baryon asymmetry of the Universe at a low energy scale, with RH neutrino masses as low as 537 GeV. This opens the possibility of probing the model in current and near-future experiments [119, 120]. We find that baryogenesis is viable for both neutrino mass hierarchies. However, in the NH case, a mass degeneracy of order $\mathcal{O}(10^{-7}-10^{-6})$ among the RH neutrinos is sufficient, whereas in the IH case a stronger degeneracy of order $\mathcal{O}(10^{-8})$ is required. Notably, in the NH scenario, even with a decay parameter as large as $\mathcal{O}(10^5)$, the correct baryon asymmetry can be achieved due to the tri-resonant enhancement of the CP asymmetry and the inclusion of flavor effects. Thus, the framework studied here is highly predictive and offers multiple avenues for experimental verification. The precise measurements of the atmospheric mixing angle θ_{23} , improved determination of CP-violating phases, next-generation $0\nu\beta\beta$ decay searches, and refined cosmological bounds on the sum of neutrino masses have strong potential to probe and possibly exclude large regions of the model's parameter space.

Acknowledgments

Tapender acknowledges the financial support provided by Central University of Himachal Pradesh in the form of freeship. The authors, also, acknowledge Department of Physics and Astronomical Science for providing necessary facility to carry out this work.

References

- [1] Q. R. Ahmad et al. Direct evidence for neutrino flavor transformation from neutral current interactions in the Sudbury Neutrino Observatory. *Phys. Rev. Lett.*, 89:011301, 2002.
- [2] F. P. An et al. Observation of electron-antineutrino disappearance at Daya Bay. *Phys. Rev. Lett.*, 108:171803, 2012.
- [3] Y. Abe et al. Indication for the disappearance of reactor electron antineutrinos in the Double Chooz experiment. *Phys. Rev. Lett.*, 108:131801, 2012.
- [4] Q. R. Ahmad et al. Measurement of the rate of $\nu_e + d \rightarrow p + p + e^-$ interactions produced by ^8B solar neutrinos at the Sudbury Neutrino Observatory. *Phys. Rev. Lett.*, 87:071301, 2001.
- [5] K. Eguchi et al. First results from KamLAND: Evidence for reactor anti-neutrino disappearance. *Phys. Rev. Lett.*, 90:021802, 2003.
- [6] Y. Fukuda et al. Evidence for oscillation of atmospheric neutrinos. *Phys. Rev. Lett.*, 81:1562–1567, 1998.
- [7] Ernest Ma. Verifiable radiative seesaw mechanism of neutrino mass and dark matter. *Phys. Rev. D*, 73:077301, 2006.
- [8] J. Racker. Mini-review on baryogenesis at the TeV scale and possible connections with dark matter. *Nucl. Part. Phys. Proc.*, 273-275:334–339, 2016.
- [9] J. Racker. Low-scale leptogenesis in the scotogenic model: Spectator processes and benchmark points. *Phys. Rev. D*, 111(8):L081301, 2025.
- [10] Thomas Hugle, Moritz Platscher, and Kai Schmitz. Low-Scale Leptogenesis in the Scotogenic Neutrino Mass Model. *Phys. Rev. D*, 98(2):023020, 2018.
- [11] Debasish Borah, P. S. Bhupal Dev, and Abhass Kumar. TeV scale leptogenesis, inflaton dark matter and neutrino mass in a scotogenic model. *Phys. Rev. D*, 99(5):055012, 2019.
- [12] Lavina Sarma, Pritam Das, and Mrinal Kumar Das. Scalar dark matter and leptogenesis in the minimal scotogenic model. *Nucl. Phys. B*, 963:115300, 2021.
- [13] Devabrat Mahanta and Debasish Borah. Fermion dark matter with N_2 leptogenesis in minimal scotogenic model. *JCAP*, 11:021, 2019.
- [14] Devabrat Mahanta and Debasish Borah. TeV Scale Leptogenesis with Dark Matter in Non-standard Cosmology. *JCAP*, 04(04):032, 2020.
- [15] J. Racker. Mass bounds for baryogenesis from particle decays and the inert doublet model. *JCAP*, 03:025, 2014.

- [16] Shoichi Kashiwase and Daijiro Suematsu. Leptogenesis and dark matter detection in a TeV scale neutrino mass model with inverted mass hierarchy. *Eur. Phys. J. C*, 73:2484, 2013.
- [17] Shoichi Kashiwase and Daijiro Suematsu. Baryon number asymmetry and dark matter in the neutrino mass model with an inert doublet. *Phys. Rev. D*, 86:053001, 2012.
- [18] Daijiro Suematsu. Baryon asymmetry and dark matter in a radiative neutrino mass model. *Nucl. Phys. B Proc. Suppl.*, 237-238:46–49, 2013.
- [19] Bikash Thapa and Ng. K. Francis. Connecting low-energy CP violation, resonant leptogenesis and neutrinoless double beta decay in a radiative seesaw model. *Nucl. Phys. B*, 986:116054, 2023.
- [20] Lavina Sarma and Mrinal Kumar Das. Phenomenology of one zero texture Yukawa matrix in a flavor symmetric scotogenic model. *Int. J. Mod. Phys. A*, 37(14):2250083, 2022.
- [21] Bichitra Bijay Boruah, Lavina Sarma, and Mrinal Kumar Das. Lepton flavor violation and leptogenesis in discrete flavor symmetric scotogenic model. 3 2021.
- [22] Tapender, Surender Verma, and Sanjeev Kumar. On lepton flavor violation and dark matter in Scotogenic model with trimaximal mixing. *Eur. Phys. J. Plus*, 140(1):43, 2025.
- [23] Tapender, Labh Singh, and Surender Verma. Dark matter and collider phenomenology in radiative Type-III seesaw model with two inert doublets. *Phys. Dark Univ.*, 50:102085, 2025.
- [24] Labh Singh, Devabrat Mahanta, and Surender Verma. Low scale leptogenesis in singlet-triplet scotogenic model. *JCAP*, 02:041, 2024.
- [25] Debasish Borah, Arnab Dasgupta, and Devabrat Mahanta. Dark sector assisted low scale leptogenesis from three body decay. *Phys. Rev. D*, 105(1):015015, 2022.
- [26] Simran Arora, Devabrat Mahanta, and B. C. Chauhan. TeV scale leptogenesis with a triplet fermion in connection to the muon $g-2$. *Phys. Rev. D*, 111(3):035004, 2025.
- [27] Tapender, Surender Verma, and Sanjeev Kumar. Implications of Trimaximal Mixing for Fermionic Dark Matter and Lepton Flavor Violation in Scotogenic Framework. *Springer Proc. Phys.*, 432:1178–1182, 2026.
- [28] Mitesh Kumar Behera, Shivaramakrishna Singirala, Subhasmita Mishra, and Rukmani Mohanta. A modular A_4 symmetric scotogenic model for neutrino mass and dark matter. *J. Phys. G*, 49(3):035002, 2022.
- [29] Shivaramakrishna Singirala, Dinesh Kumar Singha, and Rukmani Mohanta. Neutrino magnetic moment and inert doublet dark matter in a Type-III radiative scenario. *Phys. Rev. D*, 108(9):095048, 2023.

- [30] Avnish and Kirtiman Ghosh. Radiative neutrino mass with electroweak scale Majorana dark matter in the Scotogenic model. *Nucl. Phys. B*, 1002:116524, 2024.
- [31] Amine Ahriche. A scotogenic model with two inert doublets. *JHEP*, 02:028, 2023.
- [32] Debasish Borah, Satyabrata Mahapatra, Partha Kumar Paul, and Narendra Sahu. Scotogenic $U(1)_{L\mu-L\tau}$ origin of $(g-2)\mu$, W -mass anomaly and 95 GeV excess. *Phys. Rev. D*, 109(5):055021, 2024.
- [33] Simran Arora, Monal Kashav, Surender Verma, and B. C. Chauhan. Muon $(g-2)$ in $u(1)_{L\mu-L\tau}$ scotogenic model extended with vector-like fermion. *Phys. Scripta*, 98(2):025304, 2023.
- [34] Ankush, Monal Kashav, Surender Verma, and B. C. Chauhan. Scotogenesis in hybrid textures of neutrino mass matrix and neutrinoless double beta decay. *Phys. Lett. B*, 824:136796, 2022.
- [35] M. Fukugita and T. Yanagida. Baryogenesis Without Grand Unification. *Phys. Lett. B*, 174:45–47, 1986.
- [36] Sacha Davidson, Enrico Nardi, and Yosef Nir. Leptogenesis. *Phys. Rept.*, 466:105–177, 2008.
- [37] W. Buchmuller, R. D. Peccei, and T. Yanagida. Leptogenesis as the origin of matter. *Ann. Rev. Nucl. Part. Sci.*, 55:311–355, 2005.
- [38] Chee Sheng Fong, Enrico Nardi, and Antonio Riotto. Leptogenesis in the Universe. *Adv. High Energy Phys.*, 2012:158303, 2012.
- [39] Apostolos Pilaftsis. The Little Review on Leptogenesis. *J. Phys. Conf. Ser.*, 171:012017, 2009.
- [40] W. Buchmuller, P. Di Bari, and M. Plumacher. Leptogenesis for pedestrians. *Annals Phys.*, 315:305–351, 2005.
- [41] Apostolos Pilaftsis. CP violation and baryogenesis due to heavy Majorana neutrinos. *Phys. Rev. D*, 56:5431–5451, 1997.
- [42] Apostolos Pilaftsis and Thomas E. J. Underwood. Resonant leptogenesis. *Nucl. Phys. B*, 692:303–345, 2004.
- [43] Apostolos Pilaftsis and Thomas E. J. Underwood. Electroweak-scale resonant leptogenesis. *Phys. Rev. D*, 72:113001, 2005.
- [44] P. Candia da Silva, D. Karamitros, T. McKelvey, and A. Pilaftsis. Tri-resonant leptogenesis in a seesaw extension of the Standard Model. *JHEP*, 11:065, 2022.
- [45] Apostolos Pilaftsis, Pablo Candia da Silva, Dimitrios Karamitros, and Thomas McKelvey. Tri-Resonant Leptogenesis. *PoS*, CORFU2022:036, 2023.

- [46] Zhi-Cheng Liu and Zhen-hua Zhao. Renormalization group running triggered tri-resonant leptogenesis within neutrino flavor-symmetry models. *Eur. Phys. J. C*, 85(12):1387, 2025.
- [47] Bu-Yao Qu and Gui-Jun Ding. Non-holomorphic modular flavor symmetry. *JHEP*, 08:136, 2024.
- [48] Ferruccio Feruglio. *Are neutrino masses modular forms?*, pages 227–266. 2019.
- [49] T. D. Lee and G. C. Wick. Space inversion, time reversal, and other discrete symmetries in local field theories. *Phys. Rev.*, 148:1385–1404, Aug 1966.
- [50] Iris Bree, Duarte D. Correia, and Joao P. Silva. Generalized CP symmetries in three-Higgs-doublet models. *Phys. Rev. D*, 110(3):035028, 2024.
- [51] Tapender, Sanjeev Kumar, and Surender Verma. Neutrino phenomenology in a model with generalized CP symmetry within type-I seesaw framework. *Phys. Rev. D*, 109(1):015004, 2024.
- [52] Tapender, Sanjeev Kumar, and Surender Verma. Unveiling the Impact of Generalized CP Symmetry on 2HDM and Neutrino Physics. *Springer Proc. Phys.*, 361:261–272, 2025.
- [53] Priya, Simran Arora, and B. C. Chauhan. On the Generalized CP Symmetry, One Zero Texture in Neutrino Mass Matrix and Neutrinoless Double Beta Decay. 1 2025.
- [54] P. P. Novichkov, J. T. Penedo, S. T. Petcov, and A. V. Titov. Generalised CP Symmetry in Modular-Invariant Models of Flavour. *JHEP*, 07:165, 2019.
- [55] Andrei D Sakharov. Violation of cp invariance, c asymmetry, and baryon asymmetry of the universe. *Soviet Physics Uspekhi*, 34(5):392, may 1991.
- [56] Takehiko Asaka, Yongtae Heo, Takuya H. Tatsuishi, and Takahiro Yoshida. Modular A_4 invariance and leptogenesis. *JHEP*, 01:144, 2020.
- [57] Gui-Jun Ding, Stephen F. King, Jun-Nan Lu, and Bu-Yao Qu. Leptogenesis in SO(10) models with A_4 modular symmetry. *JHEP*, 10:071, 2022.
- [58] Mitesh Kumar Behera and Rukmani Mohanta. Linear Seesaw in A_5' Modular Symmetry With Leptogenesis. *Front. in Phys.*, 10:854595, 2022.
- [59] Gourab Pathak and Mrinal Kumar Das. Matter-antimatter asymmetry in minimal inverse seesaw framework with A_4 modular symmetry. 5 2025.
- [60] Monal Kashav and Surender Verma. On minimal realization of topological Lorentz structures with one-loop seesaw extensions in A_4 modular symmetry. *JCAP*, 03:010, 2023.
- [61] Simone Marciano, Davide Meloni, and Matteo Parriciatu. Minimal seesaw and leptogenesis with the smallest modular finite group. *JHEP*, 05:020, 2024.

- [62] Mitesh Kumar Behera, Subhasmita Mishra, Shivaramakrishna Singirala, and Rukmani Mohanta. Implications of A_4 modular symmetry on neutrino mass, mixing and leptogenesis with linear seesaw. *Phys. Dark Univ.*, 36:101027, 2022.
- [63] Rukmani Mohanta, Mitesh K. Behera, S. Singirala, and S. Mishra. Implications of A_4 modular symmetry on neutrino mass, mixing and leptogenesis with linear seesaw. *PoS*, FPCP2023:063, 9 2023.
- [64] Abhishek and V. Suryanarayana Mummidi. Resonant leptogenesis in inverse see-saw framework with modular S_4 symmetry. *Eur. Phys. J. C*, 86(2):116, 2026.
- [65] Dong Woo Kang, Jongkuk Kim, Takaaki Nomura, and Hiroshi Okada. Natural mass hierarchy among three heavy Majorana neutrinos for resonant leptogenesis under modular A_4 symmetry. *JHEP*, 07:050, 2022.
- [66] Priya Mishra, Mitesh Kumar Behera, Papia Panda, and Rukmani Mohanta. Type III seesaw under A_4 modular symmetry with leptogenesis. *Eur. Phys. J. C*, 82(12):1115, 2022.
- [67] Labh Singh, Monal Kashav, and Surender Verma. Minimal type-I Dirac seesaw and leptogenesis under A_4 modular invariance. *Nucl. Phys. B*, 1007:116666, 2024.
- [68] Gourab Pathak and Mrinal Kumar Das. Froggatt-Nielsen-like mechanism in the framework of modular symmetry for neutrino mass, mixing, and leptogenesis. *Phys. Rev. D*, 113(1):015015, 2026.
- [69] Jotin Gogoi, Lavina Sarma, and Mrinal Kumar Das. Leptogenesis and dark matter in minimal inverse seesaw using A_4 modular symmetry. *Eur. Phys. J. C*, 84(7):689, 2024.
- [70] Monal Kashav and Surender Verma. Broken scaling neutrino mass matrix and leptogenesis based on A_4 modular invariance. *JHEP*, 09:100, 2021.
- [71] Swaraj Kumar Nanda, Maibam Ricky Devi, and Sudhanwa Patra. Non-Holomorphic A_4 Modular Symmetry in Type-I Seesaw: Implications for Neutrino Masses and Leptogenesis. 9 2025.
- [72] Bhabana Kumar and Mrinal Kumar Das. Leptogenesis, $0\nu\beta\beta$ and lepton flavor violation in modular left-right asymmetric model with polyharmonic Maaß forms. *JHEP*, 09:071, 2025.
- [73] Priya, Labh Singh, B. C. Chauhan, and Surender Verma. Type-III seesaw in non-holomorphic modular symmetry and leptogenesis. *JHEP*, 01:036, 2026.
- [74] Salah Nasri, Labh Singh, Tapender, and Surender Verma. Dark-Portal Leptogenesis in a Non-Holomorphic Modular Scoto-Seesaw Model. 1 2026.
- [75] Asmaa Abada, Sacha Davidson, Francois-Xavier Josse-Michaux, Marta Losada, and Antonio Riotto. Flavor issues in leptogenesis. *JCAP*, 04:004, 2006.

- [76] Riccardo Barbieri, Paolo Creminelli, Alessandro Strumia, and Nikolaos Tetradis. Baryogenesis through leptogenesis. *Nucl. Phys. B*, 575:61–77, 2000.
- [77] Andrea De Simone and Antonio Riotto. On the impact of flavour oscillations in leptogenesis. *JCAP*, 02:005, 2007.
- [78] S. Blanchet, P. Di Bari, and G. G. Raffelt. Quantum Zeno effect and the impact of flavor in leptogenesis. *JCAP*, 03:012, 2007.
- [79] Steve Blanchet, Pasquale Di Bari, David A. Jones, and Luca Marzola. Leptogenesis with heavy neutrino flavours: from density matrix to Boltzmann equations. *JCAP*, 01:041, 2013.
- [80] K. Moffat, S. Pascoli, S. T. Petcov, H. Schulz, and J. Turner. Three-flavored nonresonant leptogenesis at intermediate scales. *Phys. Rev. D*, 98(1):015036, 2018.
- [81] A. Granelli, K. Moffat, and S. T. Petcov. Aspects of high scale leptogenesis with low-energy leptonic CP violation. *JHEP*, 11:149, 2021.
- [82] Takaaki Nomura, Hiroshi Okada, and Oleg Popov. Non-holomorphic modular A4 symmetric scotogenic model. *Phys. Lett. B*, 860:139171, 2025.
- [83] Hajime Ishimori, Tatsuo Kobayashi, Hiroshi Ohki, Yusuke Shimizu, Hiroshi Okada, and Morimitsu Tanimoto. Non-Abelian Discrete Symmetries in Particle Physics. *Prog. Theor. Phys. Suppl.*, 183:1–163, 2010.
- [84] C. Jarlskog. Commutator of the Quark Mass Matrices in the Standard Electroweak Model and a Measure of Maximal CP Nonconservation. *Phys. Rev. Lett.*, 55:1039, 1985.
- [85] S. M. Bilenky and S. T. Petcov. Massive neutrinos and neutrino oscillations. *Rev. Mod. Phys.*, 59:671–754, Jul 1987.
- [86] S. M. Bilenky and S. T. Petcov. Erratum: Massive neutrinos and neutrino oscillations. *Rev. Mod. Phys.*, 60:575–575, Apr 1988.
- [87] S. M. Bilenky and S. T. Petcov. Erratum: Massive neutrinos and neutrino oscillations. *Rev. Mod. Phys.*, 61:169–169, Jan 1989.
- [88] P. I. Krastev and S. T. Petcov. Resonance Amplification and θ Violation Effects in Three Neutrino Oscillations in the Earth. *Phys. Lett. B*, 205:84–92, 1988.
- [89] Jose F. Nieves and Palash B. Pal. Minimal Rephasing Invariant CP Violating Parameters With Dirac and Majorana Fermions. *Phys. Rev. D*, 36:315, 1987.
- [90] J. A. Aguilar-Saavedra and G. C. Branco. Unitarity triangles and geometrical description of CP violation with Majorana neutrinos. *Phys. Rev. D*, 62:096009, 2000.

- [91] Samoil M. Bilenky, S. Pascoli, and S. T. Petcov. Majorana neutrinos, neutrino mass spectrum, CP violation and neutrinoless double beta decay. 1. The Three neutrino mixing case. *Phys. Rev. D*, 64:053010, 2001.
- [92] Jose F. Nieves and Palash B. Pal. Rephasing invariant CP violating parameters with Majorana neutrinos. *Phys. Rev. D*, 64:076005, 2001.
- [93] S. Abe et al. Search for Majorana Neutrinos with the Complete KamLAND-Zen Dataset. *Phys. Rev. Lett.*, 135(26):262501, 2025.
- [94] Ivan Esteban, M. C. Gonzalez-Garcia, Michele Maltoni, Ivan Martinez-Soler, João Paulo Pinheiro, and Thomas Schwetz. NuFit-6.0: updated global analysis of three-flavor neutrino oscillations. *JHEP*, 12:216, 2024.
- [95] T. Hambye, F. S. Ling, L. Lopez Honorez, and J. Rocher. Scalar Multiplet Dark Matter. *JHEP*, 07:090, 2009. [Erratum: *JHEP* 05, 066 (2010)].
- [96] Riccardo Barbieri, Lawrence J. Hall, and Vyacheslav S. Rychkov. Improved naturalness with a heavy Higgs: An Alternative road to LHC physics. *Phys. Rev. D*, 74:015007, 2006.
- [97] Laura Lopez Honorez, Emmanuel Nezri, Josep F. Oliver, and Michel H. G. Tytgat. The Inert Doublet Model: An Archetype for Dark Matter. *JCAP*, 02:028, 2007.
- [98] Laura Lopez Honorez and Carlos E. Yaguna. The inert doublet model of dark matter revisited. *JHEP*, 09:046, 2010.
- [99] Ethan M. Dolle and Shufang Su. The Inert Dark Matter. *Phys. Rev. D*, 80:055012, 2009.
- [100] Laura Lopez Honorez and Carlos E. Yaguna. A new viable region of the inert doublet model. *JCAP*, 01:002, 2011.
- [101] A. Goudelis, B. Herrmann, and O. Stål. Dark matter in the Inert Doublet Model after the discovery of a Higgs-like boson at the LHC. *JHEP*, 09:106, 2013.
- [102] Maria Krawczyk, Dorota Sokolowska, Pawel Swaczyna, and Bogumila Swiezewska. Constraining Inert Dark Matter by $R_{\gamma\gamma}$ and WMAP data. *JHEP*, 09:055, 2013.
- [103] Michael Klasen, Carlos E. Yaguna, Jose D. Ruiz-Alvarez, Diego Restrepo, and Oscar Zapata. Scalar dark matter and fermion coannihilations in the radiative seesaw model. *JCAP*, 04:044, 2013.
- [104] Abdesslam Arhrib, Yue-Lin Sming Tsai, Qiang Yuan, and Tzu-Chiang Yuan. An Updated Analysis of Inert Higgs Doublet Model in light of the Recent Results from LUX, PLANCK, AMS-02 and LHC. *JCAP*, 06:030, 2014.

- [105] Agnieszka Ilnicka, Maria Krawczyk, and Tania Robens. Inert Doublet Model in light of LHC Run I and astrophysical data. *Phys. Rev. D*, 93(5):055026, 2016.
- [106] Camilo Garcia-Cely, Michael Gustafsson, and Alejandro Ibarra. Probing the Inert Doublet Dark Matter Model with Cherenkov Telescopes. *JCAP*, 02:043, 2016.
- [107] Marco Aurelio Díaz, Benjamin Koch, and Sebastián Urrutia-Quiroga. Constraints to Dark Matter from Inert Higgs Doublet Model. *Adv. High Energy Phys.*, 2016:8278375, 2016.
- [108] Alexander Belyaev, Giacomo Cacciapaglia, Igor P. Ivanov, Felipe Rojas-Abatte, and Marc Thomas. Anatomy of the Inert Two Higgs Doublet Model in the light of the LHC and non-LHC Dark Matter Searches. *Phys. Rev. D*, 97(3):035011, 2018.
- [109] Debasish Borah and Aritra Gupta. New viable region of an inert Higgs doublet dark matter model with scotogenic extension. *Phys. Rev. D*, 96(11):115012, 2017.
- [110] Benedikt Eiteneuer, Andreas Goudelis, and Jan Heisig. The inert doublet model in the light of Fermi-LAT gamma-ray data: a global fit analysis. *Eur. Phys. J. C*, 77(9):624, 2017.
- [111] Amine Ahriche, Adil Jueid, and Salah Nasri. Radiative neutrino mass and Majorana dark matter within an inert Higgs doublet model. *Phys. Rev. D*, 97(9):095012, 2018.
- [112] Ivania M. Ávila, Giovanna Cottin, and Marco A. Díaz. Revisiting the scotogenic model with scalar dark matter. *J. Phys. G*, 49(6):065001, 2022.
- [113] Daniel Foreman-Mackey, David W Hogg, Dustin Lang, and Jonathan Goodman. emcee: the mcmc hammer. *Publications of the Astronomical Society of the Pacific*, 125(925):306–312, 2013.
- [114] Caio Licciardi. The Sensitivity of the nEXO Experiment to Majorana Neutrinos. *J. Phys. Conf. Ser.*, 888(1):012237, 2017.
- [115] A. G. Adame et al. DESI 2024 VI: cosmological constraints from the measurements of baryon acoustic oscillations. *JCAP*, 02:021, 2025.
- [116] N. Aghanim et al. Planck 2018 results. VI. Cosmological parameters. *Astron. Astrophys.*, 641:A6, 2020. [Erratum: *Astron. Astrophys.* 652, C4 (2021)].
- [117] A. M. Baldini et al. Search for the lepton flavour violating decay $\mu^+ \rightarrow e^+\gamma$ with the full dataset of the MEG experiment. *Eur. Phys. J. C*, 76(8):434, 2016.
- [118] Michela D’Onofrio, Kari Rummukainen, and Anders Tranberg. Sphaleron Rate in the Minimal Standard Model. *Phys. Rev. Lett.*, 113(14):141602, 2014.
- [119] Stefan Antusch, Eros Cazzato, Marco Drewes, Oliver Fischer, Bjorn Garbrecht, Dario Gueter, and Juraj Klaric. Probing Leptogenesis at Future Colliders. *JHEP*, 09:124, 2018.
- [120] G. Anamiati, M. Hirsch, and E. Nardi. Quasi-Dirac neutrinos at the LHC. *JHEP*, 10:010, 2016.